PAPER • **OPEN ACCESS**

Charge generation by passive plant leaf motion at low wind speeds: design and collective behavior of plant-hybrid energy harvesters

IOP Publishing Bioinspir. Biomim. 19 (2024) 056003 https://doi.org/10.1088/1748-3190/ad5ba1

Bioinspiration & Biomimetics

OPEN ACCESS

RECEIVED
27 March 2024

REVISED
6 June 2024

ACCEPTED FOR PUBLICATION
25 June 2024

PUBLISHED
8 July 2024

PAPER

Charge generation by passive plant leaf motion at low wind speeds: design and collective behavior of plant-hybrid energy harvesters

Fabian Meder[1,4,*], **Serena Armiento**[1,4], **Giovanna Adele Naselli**[1], **Alessio Mondini**[1], **Thomas Speck**[2,3] **and Barbara Mazzolai**[1,*]

[1] Istituto Italiano di Tecnologia, Bioinspired Soft Robotics, Via Morego 30, 16163 Genova, Italy
[2] Plant Biomechanics Group, Botanic Garden, Faculty of Biology, University of Freiburg, Schänzlestraße 1, 79104 Freiburg, Germany
[3] Cluster of Excellence *liv*MatS @ FIT—Freiburg Center for Interactive Materials and Bioinspired Technologies, University of Freiburg, Georges-Köhler-Allee 105, D-79110 Freiburg, Germany
[4] These authors contributed equally.
[*] Authors to whom any correspondence should be addressed.

E-mail: fabian.meder@iit.it, fabian.meder@santannapisa.it and barbara.mazzolai@iit.it

Keywords: biohybrid energy harvesting, wind energy, contact electrification, triboelectric, leaf motion, plant-hybrid systems, surface charging

Supplementary material for this article is available online

Abstract

Energy harvesting techniques can exploit even subtle passive motion like that of plant leaves in wind as a consequence of contact electrification of the leaf surface. The effect is strongly enhanced by artificial materials installed as 'artificial leaves' on the natural leaves creating a recurring mechanical contact and separation. However, this requires a controlled mechanical interaction between the biological and the artificial component during the complex wind motion. Here, we build and test four artificial leaf designs with varying flexibility and degrees of freedom across the blade operating on *Nerium oleander* plants. We evaluate the apparent contact area (up to 10 cm^2 per leaf), the leaves' motion, together with the generated voltage, current and charge in low wind speeds of up to 3.3 m s^{-1} and less. Single artificial leaves produced over 75 V and 1 μA current peaks. Softer artificial leaves increase the contact area accessible for energy conversion, but a balance between softer and stiffer elements in the artificial blade is optimal to increase the frequency of contact-separation motion (here up to 10 Hz) for energy conversion also below 3.3 m s^{-1}. Moreover, we tested how multiple leaves operating collectively during continuous wind energy harvesting over several days achieve a root mean square power of ~6 μW and are capable to transfer ~80 μC every 30–40 min to power a wireless temperature and humidity sensor autonomously and recurrently. The results experimentally reveal design strategies for energy harvesters providing autonomous micro power sources in plant ecosystems for example for sensing in precision agriculture and remote environmental monitoring.

1. Introduction

The potential of and interest in sensing and robotics in applications like precision agriculture and environmental monitoring is rapidly increasing and with it the need for remote power sources. In the last years, various artificial devices, sensors, and even small robots have been designed for operation on plants and especially on leaves [1–4]. The devices may be either permanently or transiently fixed on a leaf where they perform a specific task like measuring water status and other parameters of interest [1, 5–8], consist of platforms that deliver molecules into the tissue [6, 9], and robots and drones which could use a plant or a leaf as support [6, 10–12]. Indeed, local sensors can give crucial information on plant health and microclimates.

Energy harvesting will assist in powering the increasing quantities of sensors and Internet of Things devices [13]. Especially in scenarios in which plant growth and environments needs to be monitored, energy harvesting techniques may exploit

materials and physical processes in plants to avoid the cumulative introduction of batteries that need to be recharged or replaced frequently and represent a potential environmental pollution. Indeed, plants have been used as energy sources harvesting wind [14, 15], rain drops [16], radio frequency (RF) radiation [17], the root/soil microbiome [18–20], components of plant sap [21–23], tissue temperature gradients [24], and potential differences between soil and plants [25]. In some cases (wind, rain, RF), the plant tissue is the energy converter, but others still need significant external artificial structures to perform energy conversion.

Energy conversion through contact charging is enabled by the plant tissue itself [26, 27]. Consequently, it has the advantage that it does not require specific external structures to translate wind into mechanical motion. Moreover, straightforward materials can be used to enhance the power output. The basic approach consists of thin, multi-layered artificial leaves containing a flexible electrode and a silicone layer that oscillate with the plant leaf in the wind, transiently touching each other. The silicone layer enhances contact charging, and electricity can be harvested in the artificial leaf and in the plant tissue (maximum voltage peak ≈ 150 V/impact, average voltage peak ≈20 V/impact, average current peak ≈5 μA/impact) [14, 15, 17, 26, 28]. As proof of the successful energy conversion, the plant-hybrid energy converters could transiently power over 100 LEDs by single leaves, detect wind and rain, and provide wireless sensing nodes under laboratory and outdoor conditions [14, 17, 29, 30].

However, the performance is not yet optimized as it depends on a complex interplay of factors including its mechanical motion during interaction of the biological tissue and the artificial components in the wind, the material pair that creates contact electrification (both biological and artificial parts), and the surrounding conditions among others [28].

One of the key parameters that affects energy harvesting by contact electrification is the contact area that determines possible sites for charge generation. Especially on unstructured and complex shapes it is necessary to design contact materials that have the capability to adapt and conform to each other on the macro and microscale. While this can be tuned by the materials softness and flexibility, other parameters like the ability to separate again after the contact to enable charge induction into the electrodes, and the complex behavior in fluid flow also play an important role that require investigation. Moreover, to increase the power output, it is desirable to harvest from multiple leaves simultaneously. This collective harvesting mode yet requires that electrical impulses from different leaves in the same plant interact constructively and it needs to be tested to which extend collective energy harvesting is possible.

Here, we investigate how the design of artificial leaves affects the output performance of plant-hybrid energy harvesters based on *Nerium oleander*. The leaf blade stiffness is a key factor affecting the dynamic response and we changed the artificial leaf's stiffness here intuitively to gain insights in the expectedly complex coupled motion behavior. Additionally, we investigated how blade flexibility influences the apparent contact area and subsequent contact charging during interactions between the plant and artificial leaf. The daily mean wind speeds in Europe are typically below 3–4 m s^{-1} especially on lower heights (e.g. 10 m above ground level) [31] and leaves show significant motion already at 1 m s^{-1} [32]. Thus, four designs leading to different dynamic responses have been assembled, installed on *N. oleander* leaves and exposed to low wind speeds of up to 3.3 m s^{-1} in a phytochamber equipped with a tunable wind tunnel; energy conversion and leaf motion were tracked. We then tested how electrical impulses created simultaneously in the same plant may affect the energy harvesting with multiple leaves and exposed the devices for several days to continuous wind. Finally, by a plant with eight artificial leaves we could successfully power a remote temperature and humidity sensor and wireless transmitter reporting data to a receiver. The results are an important step towards optimized artificial leaves fabricated of straightforward materials to translate passive leaf motion into electricity and, more generally, how to adapt artificial components to unstructured biological systems. The capability of directly powering a remote sensor shows the potential as a new tool for energy-autonomous environment, microclimate, and plant monitoring.

2. Results and discussion

2.1. Artificial leaf design and rationale

All artificial leaves are designed to be fixed at the petiole of a *N. oleander* leaf so that the blade freely moves on the natural leaf's blade to produce transient contact and separation motion from the leaves' passive motion in wind. This leads to contact electrification and electrostatic induction of the charges into the tissue and artificial leaf electrode that then can be harvested as electrical energy. Starting from the original design reported in previous studies ([14, 15]) we have proposed three new designs and compared them with the original one.

Figure 1 shows the different designs and their main characteristics. The original design and Design 2 consist of a 200 μm PET layer with a ∼50 nm indium tin oxide (ITO) electrode and a 500 μm silicone layer. However, an additional notch hinge was cut in the leaf blade of Design 2 to introduce an additional degree of freedom of movement in the blade that is expected to help to increase the compliance and contact area with leaves that are typically

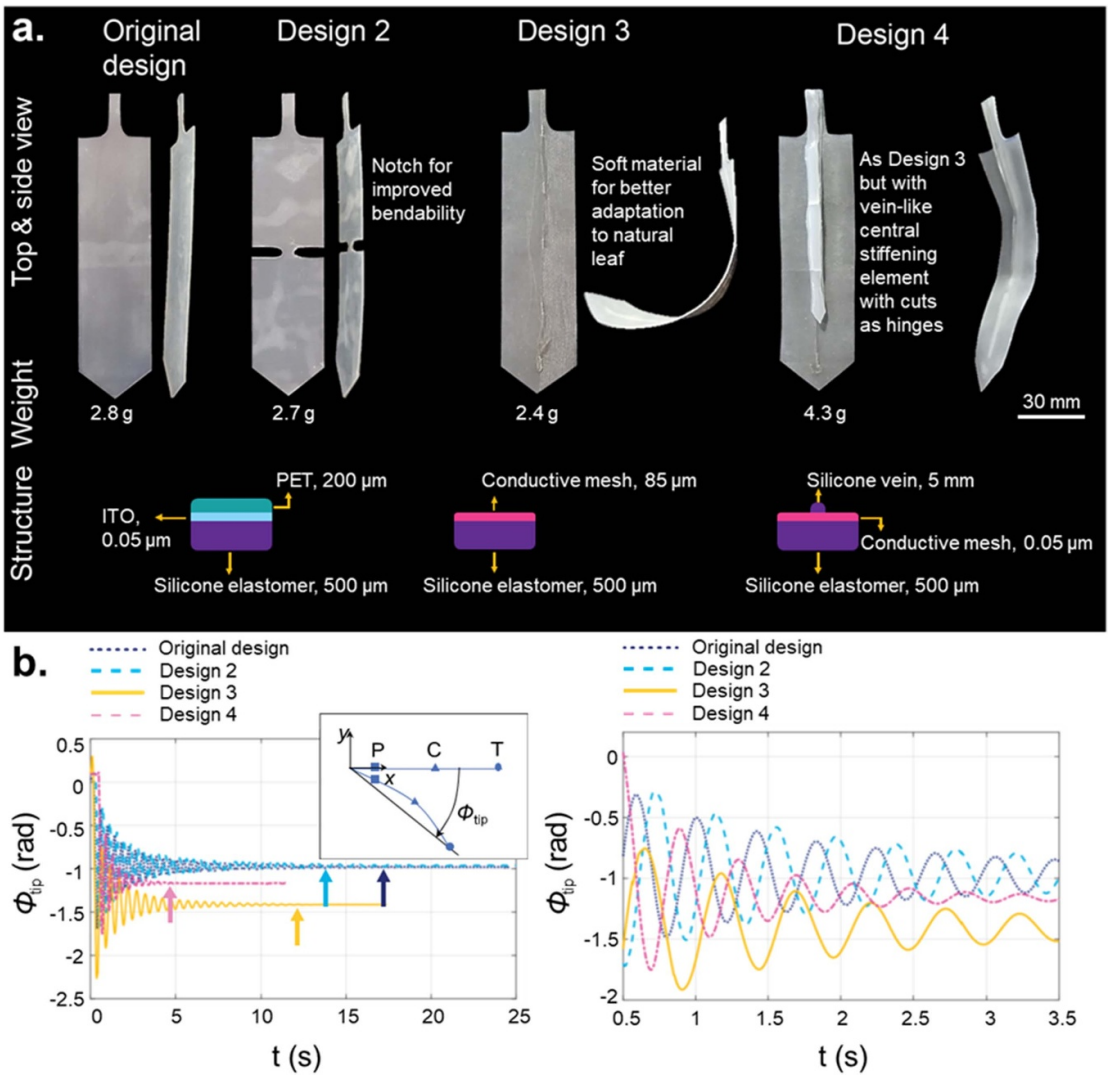

Figure 1. Overview of the four investigated artificial leaf designs to be installed on the plant leaf for enhancing surface contact electrification and energy conversion. (a) Photos, properties, and a schematic of the cross-sectional composition and components of the multilayered structure. Video 1 (see supplementary material) shows the different designs and their deformation capabilities. (b) Different oscillations of the artificial leaves obtained by motion tracking. The petiole was fixed and the leaf held in a horizontal position by a support, then the support was removed, leaving the leaf to freely oscillate until it reached static equilibrium. Points P, C and T denote the transition from petiole to lamina, the center point and the tip of the lamina, respectively. Left panel: Rotation angle ϕ_{tip} of the tip of the artificial leaves vs. time t, measured negative as indicated by the arrow, tracking point T. The colored arrows indicate the timepoint at which oscillations have not been detected anymore for the different prototypes. Right panel: for clarity, the panel shows the same curves in the interval $[0.5,\ 3.5]$ s. The legend refers to both plots. Figure S2 shows data for tracking of point C in comparison to T.

slightly curved and not perfectly straight. In Design 3 and 4 instead, the more rigid ITO-PET electrode was replaced by a softer, 85 μm thick, nickel and copper-coated polyester conductive mesh to give the leaf blade more flexibility and thus further possibility to adapt its shape during a contact to the shape of the plant leaf (electrostatic induction in either ITO or conductive mesh is comparable as detailed in figure S1). On the bottom, a 500 μm silicone layer was glued as the material contacting the leaf blade as in the original design and Design 2. Design 4 has in addition a leaf vein-like central stiffening element (10 cm length, 5 mm diameter) with two cuts in distance of 3 cm to allow bending of the blade downwards while limiting upwards bending. Video 1 shows the different designs and visualizes their different deformation capabilities.

To compare the four designs based on stiffness and damping, we tested all the leaves as in our previous work [28]. The end section of the petiole was fixed by a clamp and the leaf held by a support in a horizontal position. Then, the support was removed, leaving the leaf to freely oscillate until it reached static equilibrium. We recorded the oscillations using a high-speed camera and analyzed it by means of three markers placed on the leaf: at the tip, at the center, and at the free end section of the petiole. Taking the clamped section as the origin of a system of coordinates having x-axis oriented horizontally and y-axis vertically (pointing upward),

the trajectory of each marker, assumed to be planar, is obtained by video tracking as described in the methods as a series of ordered pairs $(x(t), y(t))$. Figure 1(b) shows the rotation angle spanned by the tip of the generic leaf during the oscillation, which is calculated as $\phi_{\text{tip}} = \tan^{-1}(y/x)$ at each sampling time t. The data displayed in all figures is freely available [33].

The results show that the tip oscillations of original design and of Design 2 exhibit similar dynamics. However, their behaviors differ at point C, due to the notch in Design 2 (see supplementary figure S2). As expected, Design 3 turns out to be the softest. In fact, at the static equilibrium, the angle reached is almost $\pi/2$, while the other leaves deflect less. In particular, Design 4 achieves a smaller deflection despite being heavier than Design 3. That is due to the stiffening midvein-like central structure. However, such addition also influences the amount of energy dissipated during the oscillation. Design 4 expectedly reaches the static equilibrium faster than the other leaves, meaning that it is characterized by a relatively high structural damping compared to the other designs. In general, we suppose that increasing the oscillation frequency leading to a higher number of contacts would increase the energy output of our harvesters. Yet, another aspect is the 'quality of the contact' in terms of how many charges are created per single contact event. This depends likely on the effective contact area the structure makes with the leaf, and this depends on the deformation of the leaf blade (including out-of-plane deformation). We assume that a softer structure will adapt better to the natural leaf surface causing more potential contact points. Even if our work below approaches these aspects, further investigations are required to better understand the complex correlation between leaves oscillations, charge generation, the plant motion, and energy outputs.

2.2. Apparent contact area between artificial and N. *oleander* leaves

A key parameter for energy conversion by contact electrification is the contact area between the two surfaces as it defines the locations of possible charge transfer through contact electrification. To estimate the influence of the leaf blade designs on the apparent contact area when interacting with the *N. oleander* leaf, static dropping experiments have been conducted in which the transfer of a fluorescent paint at the contact sites was measured. The procedure is illustrated in detail in figure S3(a). After coating the artificial leaf's blade homogenously with the fluorescent paint, the artificial leaf was fixed on the petiole of the natural leaf as in the final application circumstances. Then its tip was lifted to a height of 7 cm and subsequently dropped onto the plant leaf. This results in the transfer of the fluorescent paint to the leaf blade and visualizes areas of possible contact regions and indicates areas were no contact occurred. As the leaf morphology varies slightly from leaf to leaf, ten individual leaves from three different plants have been tested with all 4 designs each. Figure 2(a) shows the workflow and example images of the transferred fluorescent paint used to calculate the apparent contact area during the dropping tests (all analyzed images are available in figure S3(b)).

The results clearly indicate that the leaves with softer leaf blades and higher degrees of freedom for multidirectional deformation (Designs 3 and 4), lead to ∼3 times higher apparent contact areas (on average ∼9.9 and 8.6 cm^2/leaf, respectively) compared to the original design (∼2.8 cm^2/leaf). In addition, the central hinge of Design 2 leads to a slightly increased contact area (∼4.2 cm^2/leaf) as well suggesting that increasing the blade flexibility increases potential contact regions. Figure 2(c) shows a radial heat map that illustrates the contact areas of the different designs for each individual leaf tested. It confirms that highest values are typically achieved with Design 3. Indeed Design 4 shows on leaf A and C a smaller contact area than Design 3. This reduction is likely due to the re-stiffening by the artificial mid-vein and not due to the additional weight, which may rather support a higher impact force leading to better adaptation of the flexible blade to the leaf surface during the as-described dropping tests. The detected apparent contact areas only indicate the areas in which real contact regions that lead to charging occur in higher probability. The real contact sites have likely micro and nanoscale dimensions and their quantity and microscopic location, as well as contact pressure are of course not analyzed here. Such measurements are especially difficult for complex systems with hierarchical structures such as leaves for which currently no method exists. Yet, the macroscopic results clearly show that, expectedly, softer and more flexible structures adapt better to the different leaf shapes, as shown in figure S3(b), leading to larger apparent contact regions. Nevertheless, the structure's flexibility has likely further effects, especially on the aerodynamic behavior of wind-driven leaf motion as described below.

2.3. Voltage generation as function of artificial leaf design

Figure 3(a) summarizes the peak voltages obtained by the artificial leaves installed on a *N. oleander* plant exposed to a controlled wind source operating in crossflow orientation with the leaf as shown in figure 3(b) and measured between the leaf tissue and the electrode in the artificial leaf.

A crossflow orientation has been implemented as it has previously led to highest energy conversion and power outputs [14]. Measurements of the generated currents (up to 1.2 μA), the transferred charges (up to 5 nC), and peak power (up to 60 μW) are reported in figures S4, S5 and S6, respectively and show similar trends to the voltage signals in detail discussed

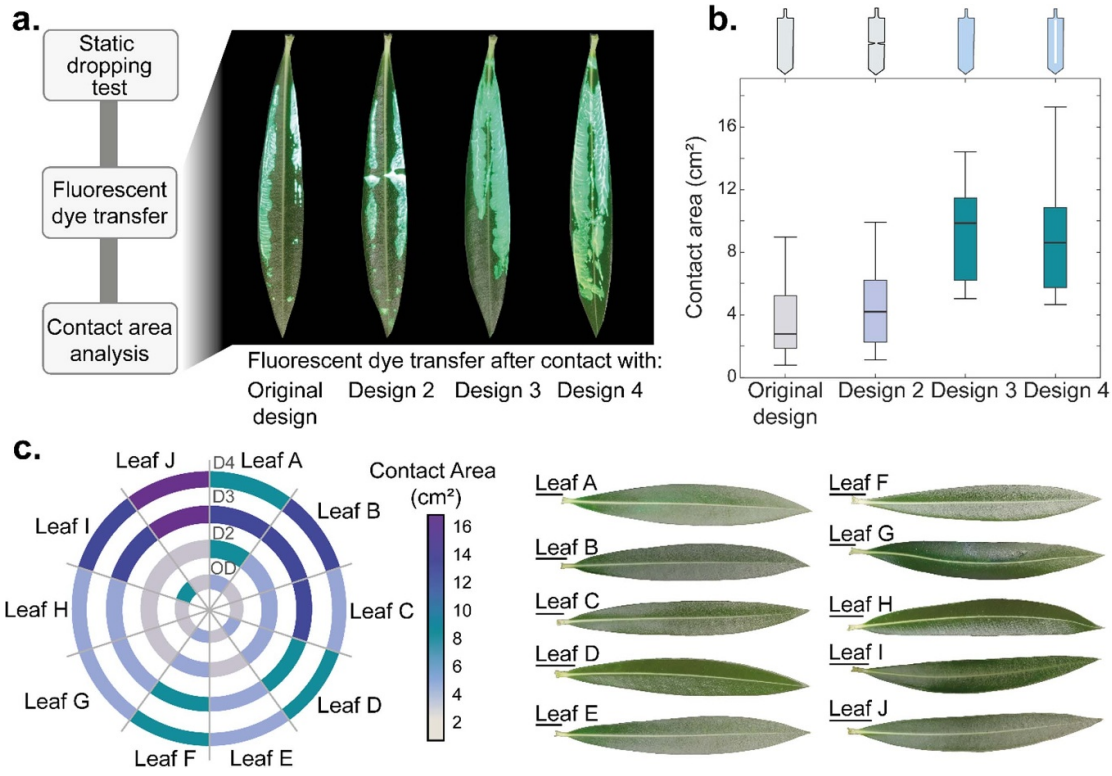

Figure 2. Estimate of the contact areas caused by artificial leaves when interacting with *N. oleander* leaves. (a) Block diagram for the estimation of the contact areas. The areas in which the fluorescent dye has been transferred indicate the areas with higher contact probability. Further details on the analysis are given in figure S3. (b) Boxplot illustrating the analysis of the contact area over ten *N. oleander* leaves as function of artificial leaf design (the boxes upper and lower edges indicate the 75th and 25th quartile respectively, the central line indicates the median value the bars indicate the minimum and maximum values). The icons on top of the graph illustrate schematically the main differences between the designs. (c) Radial heat map illustrating the variability in contact area of each design (represented as a circle) with each tested leaf (represented as a segment of each circle). Less saturated colors indicate lower contact area compared to more saturated colors. The photos of the tested *N. oleander* leaves represent the variability of leaf shape and dimension (scale bars = 2 cm).

below. Temperature and humidity in the phytochamber were kept at 23 °C and 55%, respectively during the tests. Figure 3(a) shows that the voltage generated by the original design has an almost linear correlation with the wind speed reaching a maximum of 54 ± 13 V at the highest measured wind speed of 3.3 m s^{-1}. This wind speed is characterized by the Beaufort scale as a 'light breeze' and significant voltages above 50 V can be achieved even at lower wind speeds. A similar behavior is observed for Design 2 reaching a maximum of 45 ± 11 V at 3.3 m s^{-1}. This is slightly lower compared to the original design but voltages for 1.4 and 2.2 m s^{-1} are higher with 26 ± 9 V and 43 ± 11 V, respectively. This could be an effect related to the increased contact area obtained with Design 2. Nonetheless, at higher wind speeds the additional hinge seem to be somewhat disadvantageous although the effect is not severe. The small decline observed for Design 2 at higher wind speeds may be due to an additional torsional motion around the hinge in the center of the leaf blade as seen in video 2.

A notably different behavior is found for Designs 3 and 4. While Design 3 obtains the highest voltage, 71 ± 23 V at 3.3 m s^{-1} of all prototypes analyzed, both, Design 3 and 4 generate lower voltages at wind speeds below 3.3 m s^{-1} compared to the original design and Design 2. Moreover, Design 4 even reaches at 3.3 m s^{-1} only 36 ± 7 V. Figure 3(c) compares all designs in a diagram in which the height of a petal shows the average voltage while the width represents the standard deviation of the voltage signals. Design 3 clearly performs best at 3.3 m s^{-1} and this is probably caused by the increased contact area achieved by its multidirectional flexibility.

Nevertheless, although higher contact areas have been achieved with the Design 3 and 4, at lower wind speeds, the original design and Design 2 outperform the other designs. This is furthermore confirmed by the frequency in which voltage peaks appear at 1.4 and 3.3 m s^{-1} as shown in figure 3(d). The frequency of voltage peaks depends on the oscillation of the leaf blades in the wind and correlates with the number of mechanical contacts that lead to a significant charge formation [14, 15]. Expectedly, a higher frequency increases the output performance. A comparison of voltage peaks and contacts measured by high-speed camera recordings is given in

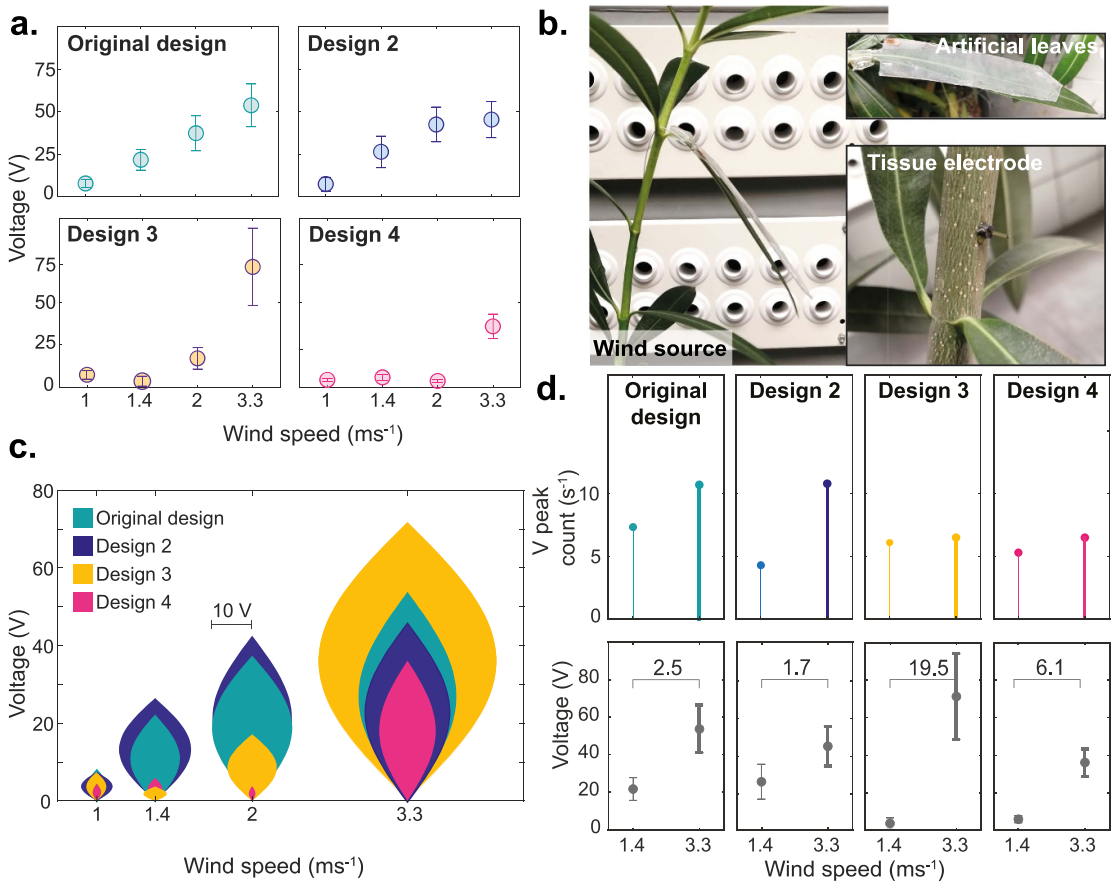

Figure 3. Electrical output as function of wind speed and artificial leaf design when converting passive motion of a *N. oleander* leaf into electricity. (a) Peak voltages as function of artificial leaf design and wind speed (current measurements, transferred charges, and peak power are given in figures S4, S5, and S6 respectively). Data points represent average and standard deviation of typically ∼90 voltage peaks. (b) Image of the experimental setup in which a single artificial leaf was installed on the *N. oleander* leaf and exposed to varying wind speed in a specialized phytochamber (T 22 °C, RH 55%). The inset shows the tissue electrode at which charges generated on the leaf were recorded. (c) Summary of the peak voltage measurements of all designs and wind speeds using a petal plot. The height of each petal is the average amplitude of the voltage signals while the width (scalebar 10 V) represents the standard deviation of the data; each color represents a different design. (d) Frequency of voltage peaks (which correlates to the frequency of contacts) at 1.4 and 3.3 m s^{-1} for all designs in comparison with the voltage peaks (numbers above the braces in lower panel indicate the difference in voltage magnitudes among the two wind speeds).

figure S7. Highest frequencies of 10.7 and 10.8 peaks per second, respectively are observed for the original design and Design 2, whereas Design 3 reaches the highest voltage at 3.3 m s^{-1}, the frequency is only 6.5 peaks/s. The same is also observed for Design 4 (6.6 peaks/s).

High speed video recordings (video 2) suggest that the origin of the decreased contact frequency is the increased flexibility that permits multidirectional motion and does not necessarily force the leaf after separation towards another contact with the *N. oleander* leaf. Instead, it leads to a turbulent dynamic motion with significant torsional elements that could promote separation of the two blades. An increased separation was observed mostly for Design 4, in which the reinforcing central vein-like element in combination with the highly flexible leaf blade may, in crossflow direction, bend upwards which leads to a buoyancy and separation between the blades despite the increased weight and central stiffening. The expectedly complex aeroelastic behavior of the combination of a biological and artificial system renders the design of a structure that increases, both contact area and contact-separation frequency under wind excitation more challenging. Moreover, the interaction between the fluid and the leaf is challenging to derive from our experiments. Also, the coupling between the plant leaf and the artificial leaf, and the effects of branch and stem motion should be considered. Hence, a more complex study would be necessary. This is certainly interesting for improving the artificial leaf design and energy harvesting capability but goes beyond the current study.

However, our results show that it is indeed possible to optimize the overall performance by artificial leaf's petiole and blade design. A combination of increasingly flexible and stiffer regions as in Design 2 probably results in best performance at multiple wind speeds. Future work should thus focus on an optimal combination of flexible elements and stiffer structures that reinforce contact-separation next to overall weight. On the other hand, structures like

Design 3 may be created that specifically produce significant voltages only above a certain wind speed, presenting to some extent an embodied sensing/control function. Although further tests may be required on this, we believe that the artificial leaves remain functional also at higher wind speeds and do not damage the plant. Artificial leaves with the stiffest 'Original design' have been tested in a different study also at higher wind speeds of up to 7 m s^{-1} and remained functional [14] and *N. oleander* leaves have been shown to support 200 times their own weight and we expect that damage caused by artificial leaf's additional weight are unlikely [28]. By cutting the artificial leaves into different shapes and adapting weights, for example by decreasing the thickness of the silicone layer, the leaves can be adapted to other plant species as well [14].

Regarding the biological component, wind-driven plant leaf oscillations are itself still an ongoing research field with many open questions and new insights would help in developing the artificial leaves and other biohybrid and bioinspired systems for wind energy harvesting. The leaves' inclination is another interesting parameter that has yet not been investigated in detail. It may change from leaf to leaf for example with leaf size and weight and tissue hydration. We suggest that it may influence the gravitational-driven downward motion of the artificial leaf towards the natural leaf after a wind-driven separation and hence affect contact forces and it should be analyzed in a dedicated study to further understand its role and effect on the plant-hybrid energy harvesting approach.

A comparison with a purely artificial triboelectric wind energy harvester, for example with the interesting work from Zhao *et al* [34] reveals that assuming a similar total area (Zhao: 5000 mm^2, ours: 3600 mm^2) and comparable contact frequency of 10–20 Hz, our harvester lead to similar or slightly higher peak voltages (Zhao: 20 V, ours: 35 to up to 75 V at wind velocities between 3–4 m s^{-1}). Although a broader comparison with other triboelectric wind energy harvesters would be interesting, this is challenging as data on the performance of the devices at low wind speeds $<$3–4 m s^{-1} is often lacking.

2.4. Effect of simultaneous signals from multiple leaves occurring in the same plant

It was shown earlier that energy harvesting with multiple artificial leaves can enhance the total charge yield to be harvested and enable to harvest wind from multiple directions [14, 15]. However, it is unclear what happens when electrical signals created at different leaves are transported simultaneously in the plant tissue. Thus, before using the original design and Design 2 for continuous energy harvesting (section 2.5), we aimed to approach a crucial question that is, how signals from different leaves interfere when induced into the same conductive tissue. In other words, when two alternating current signals are generated in or out of phase on two different leaves that connect to the same conductor (same plant tissue), what is the resulting signal that is measured at the common tissue electrode?

An experiment with controlled touch stimuli of multiple leaves on the same plant has thus been conducted. We created a platform which allowed touching two leaves of the plant with two independently addressable linear actuators with a controlled force. The actuators are driven by a tailorable sinusoidal waveform input signal. It was thus possible to stimulate two leaves of the same *N. oleander* controlling the actuators' input signal in phase, with a phase shift, and out of phase (the concept is schematized in figure 4(a)).

Figure 4(b) shows the current recordings at the common tissue electrode. First, the current signals of the left and right actuator have been recorded separately and then simultaneously with 0°, 90°, and 180° phase shift, respectively (frequency of 5 Hz, 0.5 N impact force, 25 mm^2 stimulation area, silicone elastomer as stimulus material). The distance of the actuated silicone elastomer sample and the leaf surface is plotted (lower set of graphs) as tracked from high-speed video recordings of the experiments (video 3).

The signals from the left and right actuator (stimulating leaf 1 and 2 as shown in figure 4(b), with 5 signals provided as examples) prove the generation of comparable alternating current signals, with amplitudes of 0.17 $\pm$ 0.02 μA and 0.21 $\pm$ 0.02 μA, respectively (average and standard deviation from 40 measurements). Negative peaks are generated during approach/contact, the positive peaks during separation. When both actuators are then used simultaneously without a phase shift, the two actuators hit the two leaves in the same moment and the signal consequently augments. That agrees with the fact that an increase in the contact surface area expectedly increases charge generation [26]. When a 90° phase shift is applied, the two actuators touch sequentially the leaves and separate from the surface subsequently, one after the other (video 3 shows the behavior). This leads to two negative peaks (generated during approach/contact) followed by two positive peaks (generated during separation) with peak amplitudes that are slightly higher but comparable to the single stimuli. When the 180° phase shift is applied, the positive and negative signals are expected to appear at a very similar time. Indeed, ten peaks in one second (resulting from two 5 Hz stimuli) can be observed with a positive and a negative component appearing in a time distance of $\sim$10 ms with peak amplitudes about a little bit less then those of the single stimuli. Thus, even in a very synchronized inverse stimulus controlled by the 180° shifted sinusoidal control (and confirmed by the highspeed videos, video

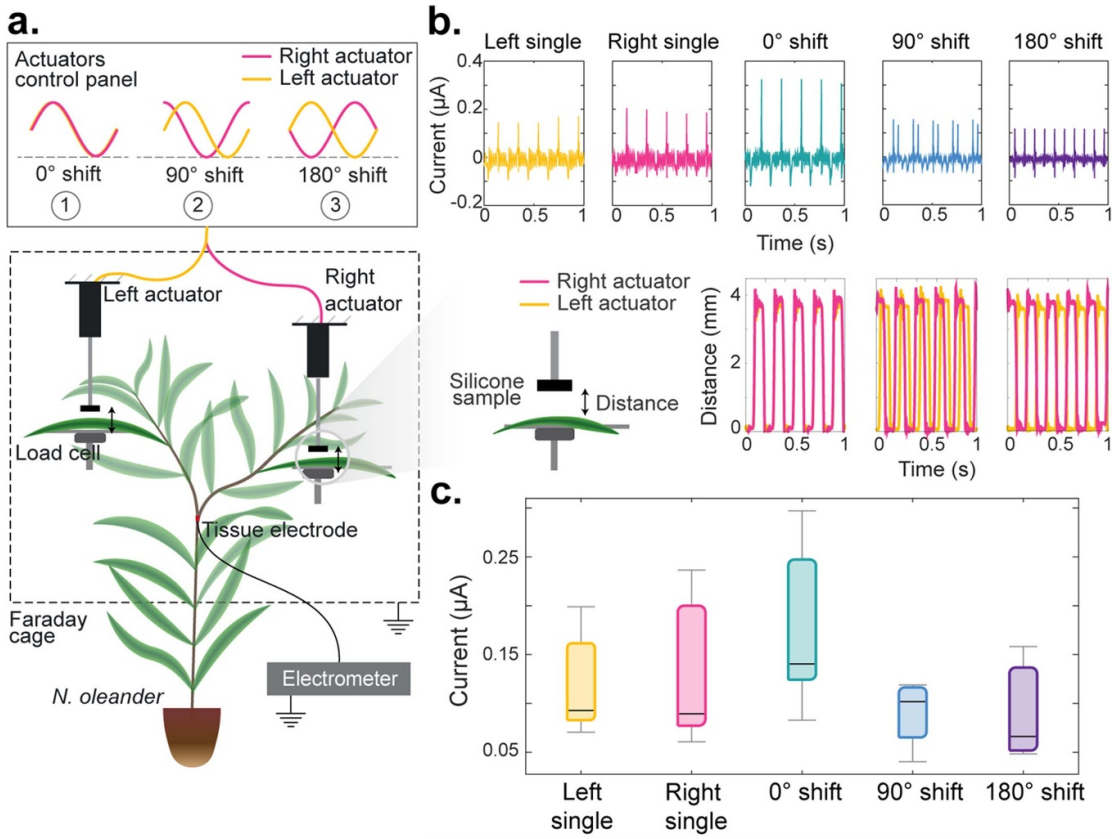

Figure 4. Controlled generation and tracking of current signals from multiple artificial leaves in the same plant. (a) Schematic of the experimental setup and control of the two actuators touching two individual leaves on the same *N. oleander* plant. (b) Current peaks recorded at the common electrode in the plant tissue. Upper panel: single (yellow and pink curve) and simultaneous stimuli with given phase shifts (green, blue, and purple curves). Lower panel: the motion of the right (pink) and left actuator (yellow) and their distance from leaf surface tracked from high-speed video recordings (video 3, see supplementary material). (c) Comparison of the average magnitude of current peaks and standard deviations of typically ∼85 peaks obtained under the given stimuli.

3), the signals can be observed separately. This can be explained by the relatively short peak duration (typically less than ∼20 ms full width at half maximum) that is brief enough to allow even for multiple stimuli creating positive and negative signals almost simultaneously (a situation that is rather unlikely during unsynchronized wind excitation), and consequently both signals can still be measured (and thus harvested) instead of cancelling out. This confirms also a theoretical model presented earlier [17]. The experiments furthermore confirm that energy harvesting with multiple leaves on the same plant is possible and will augment the power output.

2.5. Continuous energy harvesting and demonstration of sensing application

To demonstrate the capability to continuously supply a wireless sensor node by multiple artificial leaves on the same plant, eight artificial leaves (Design 2) were fixed on a *N. oleander* and exposed to continuous wind at 3.3 m s^{-1} in the specialized phytochamber as shown in figure 5(a). The measurement circuit is indicated in which all leaves feed a single storage capacitor connected to the common trunk electrode and to individually rectified electrodes of the artificial leaves.

First, we characterized the continuous charging of a 136 μF capacitor measuring the charges transferred to the capacitor at a wind speed of 3.3 m s^{-1} (figure 5(b)). Capacitor charging kinetics at 0, 1.4, and 3.3 m s^{-1} are given in figure S8. When the capacitor reached a voltage of 2 V or ∼270 μC transferred charges, it was automatically discharged by the acquisition platform. The graph shows that continuous charging is possible even over more than 45 h and that the variation of the transferred charges over time ($dQ_{transferred}$) remains nearly unchanged and even slightly decreases in this period. This indicates that, given an adequate wind speed, the eight artificial leaves of Design 2 provide together a repeatable charge quantity. Further aspects such as a changing environmental humidity may affect the charge transfer. However, the effect is typically reversible as shown in figure S9 where high humidity of 80% was switched to 50% showing a recovery of the charge transfer rates.

We then calculated the root mean square (RMS) power of each corresponding charging cycle (P_{RMS},

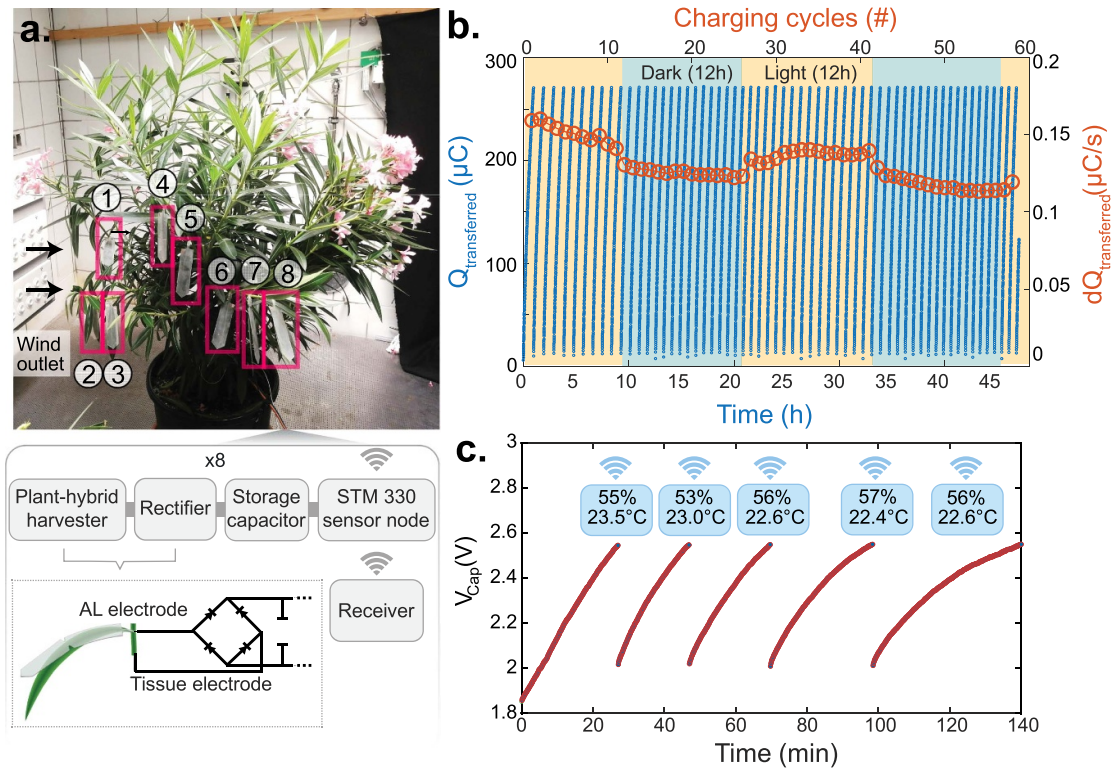

Figure 5. Demonstrating energy harvesting by multiple leaves and the potential for sensing applications. (a) Image of a *N. oleander* with eight artificial leaves (here original design) in crossflow orientation to the wind source during energy harvesting experiments with multiple leaves. The schematic on the bottom illustrates the energy harvesting circuit as well as the connections of the artificial leaf and plant inner tissue to the external electronics. (b) Kinetics of charges transferred to a 136 μF capacitor during 48 h of continuous operation of a *N. oleander* with eight artificial leaves (Design 2) at a windspeed of 3.3 m s^{-1} (T 22 °C, RH 55%). (c) Operation of a wireless sensor node powered solely by the 8 artificial leaves (original design) when subject to wind (3.3 m s^{-1}).

see figure S10(a)) which resulted in an average of 6.0 $\pm$ 0.6 μW and compare it to electronic devices like sensors and wireless transmission protocols in Figure S10b using a recent overview of Pecunia *et al* [35].

Next, a wireless temperature and humidity sensor node was connected to the capacitor and the charging characteristics as well as the sensor's ability to measure were studied using an *N. oleander* modified with eight artificial leaves (original design, circuit given in figure 5(a)). The voltage over the common storage capacitor connected to the sensor node and the transmitted temperature and relative humidity (RH) measurements are given in figure 5(c). To perform a measurement and transmit cycle, the 136 μF capacitor needed to reach a voltage of ~2.6 V. A measurement and transmit cycle then reduced the voltage to ~2 V indicating that a charge quantity of ~82 μC was required to perform the task. Another sensing cycle then required recharging from ~2 V to ~2.6 V. Under continuous wind of 3.3 m s^{-1} and eight artificial leaves, the plant-hybrid generator powered the sensor node once every ~30–40 min and sent the data packages containing the local temperature and humidity which correspond to the values controlled in the phytochamber (22 °C, 55% RH) to an external receiver.

3. Conclusions

We have tested 4 artificial leaf designs with variable mechanical properties in terms of their capability to harvest electrical energy from passive leaf motion in wind using contact electrification between the surfaces of the plant and the artificial leaf and electrostatic induction into the tissue and an electrode integrated in the artificial leaf. Our results show that passive motion of plant leaves can be converted into electrical charges that can be used to repeatedly power wireless sensor nodes with relatively low wind speeds of 3.3 m s^{-1} achieving charge transfer of over 250 μC, data transmission every ~30–40 min, and an RMS power of 6 $\pm$ 0.6 μW. This furthermore proves the potential to use leaves as autonomous micropower source for sensor nodes. Moreover, collective harvesting from multiple leaves increases the power output. Especially in environmental or microclimate monitoring it could be interesting to gather information on the wind speed and artificial leaves may be designed to create certain voltage patterns at specific wind-speeds. Importantly, our results show that the performance across different wind speeds are affected by the artificial leaf design, its flexibility, its oscillation frequency, its adaptation to the plant leaf and the apparent

contact areas as well as the aeroelastic behavior during wind motion. We currently recommend Original Design and Design 2 for better performances as the softer Designs 3 and 4 have a more complex aerodynamic performance despite higher peak voltages. Consequently, further improvements in the electric output must be achieved by tuning these parameters together with other aspects like the chemical nature of contact materials and the surface structure of the artificial leaves additionally affecting contact electrification and energy conversion.

4. Materials and methods

Fabrication of artificial leaves: To fabricate the original artificial leaves [14] and Design 2, transparent ITO-coated PET films (thickness 200 μm, nominal sheet resistance 350–500 Ω per square) were purchased from Thorlabs Inc., USA. Design 3 and Design 4 were fabricated using a conductive mesh made of polyester coated with nickel and copper (thickness 85 μm, surface resistivity $<$13 Ω per square), purchased from Holland Shielding Systems BV, The Netherlands. A thin layer of silicone rubber adhesive (Sil-Poxy^{TM}, Smooth-On Inc., USA) was applied on the ITO-layer or conductive mesh. In the conductive mesh a single stainless-steel wire was previously sewn in which was used to connect the conductive mesh to the cable for harvesting. Subsequently, a layer of translucent silicone rubber was added (thickness 500 μm, Modulor GmbH, Germany, washed with isopropyl alcohol and dry wiped). After drying for 24 h, the layers were cut into the desired shapes using a laser cutter (VersaLaser VLS3.60, Universal Laser Systems Inc., USA). All cutting edges were sealed with silicone. The leaves were attached onto the petioles of the natural leaves for further analysis and energy harvesting.

Plants: Four *Nerium oleander* bushes (height ∼70 cm, diameter ∼100 cm) were provided by the Botanic Garden, University of Freiburg, Germany. The plants were watered daily and kept in a phytochamber with lighting in a 12 h day and 12 h night cycle.

Phytochamber and wind source: The plant-hybrid energy harvesters have been exposed to controlled air flow in a specialized phytochamber (height: 2.13 m, depth: 2.75 m, width: 2.5 m) equipped with an active climate control system and a wind source consisting of 96 individually adjustable nozzles that were oriented towards the plant which was placed at a distance of ∼30–50 cm from the nozzles (measured from the plant center). A ventilation system (MUB 042-500DV-A2, Systemair, Skinnskatteberg, Sweden (max speed: 1330 rpm)) in combination with a frequency converter (VLT® HVAC Drive FC 102, Danfoss, Nordborg, Denmark) was used to control the wind speed. The wind speed at the plant was measured with a hot wire anemometer (405i, Testo SE & Co. KGaA, Germany). During all measurements, illumination was kept constant (12 h day/12 h night cycle) and the temperature was kept at 22 ± 1 °C. The RH was typically 50% ± 3% or varied between 30% and 70% RH as indicated in the figures. Temperature and humidity were continuously monitored using a humidity and temperature data logger (EL-USB-2+, Lascar Electronics Ltd, Whiteparish, UK).

Estimation of the apparent contact area: Static dropping tests have been performed in which a freshly picked *N. oleander* leaf was firmly fixed together with an artificial leaf at their petioles using a clamp on a stand. The silicone layer on the artificial leaf was previously coated with a thin layer of fluorescent paint (Silc Pig™ Electric Yellow, Smooth-On, USA) using a squeegee. Then the artificial leaf was lifted to a height of 7 cm from the *N. oleander* leaf and left to drop onto the plant leaf. The procedure was repeated three times, then the *N. oleander* leaf was removed from the holder and illuminated at a wavelength of 365 nm and photographed. The areas covered by the fluorescent paint on the leaf were analyzed using ImageJ, version 1.54 g.

Electrical measurements: Voltages, currents, and transferred charges were measured with an oscilloscope (MSO7014A, Agilent Technologies, USA) and a high input impedance electrometer (6517B, Keithley, USA). Capacitor charging was performed using a data acquisition circuit with eight individual ceramic capacitors (136 μF, Taiyo Yuden Co. LTD, Japan) connected to a diode bridge connected to the common tissue electrode and the eight artificial leaves that have been individually rectified with a diode bridge each. The circuit records the voltage across the individual capacitors and discharges the capacitors when a certain set threshold voltage (typically 2 V in our experiments) is reached.

Platform for double stimulation: Controlled mechanical stimulation of multiple leaves was achieved by modifying a self-made apparatus that has been described earlier [26]. In short, two linear actuators (4 Ω HiFi fullrange driver, diameter 8 cm, model FRS, Visaton, Germany) were driven by a, high-voltage/high-current operational amplifier (OPA549T, Texas Instruments, USA) and controlled by a function generator (established using a CY8CKIT-059, Infineon Technologies AG, Germany) was used to apply vertical motion selecting waveform and adjusting phase shifts between the two actuators, controlling also frequency, amplitude, and offset. A piece of silicone elastomer (25 mm^2) was installed on a sample holder attached to the two actuators each and placed parallel above two leaves at a distance of ∼60 cm on the same plant. Underneath the leaves, a z-stage with a 1 N load cell (SEN-14727, SparkFun Electronics, USA) acquired by a load cell amplifier (SF-SEN-13879, Sparkfun Electronics, USA) was mounted to monitor the impact force that

was maintained during the experiments at 0.5 N by adjusting the distance between the z stage and the actuated silicone sample. Electric signals were measured at a gold-coated pin electrode placed in the trunk in contact with the internal tissue at a distance of ∼30 cm from the leaves, either using an electrometer or the oscilloscope.

Wireless sensor node: The wireless sensor was realized using the temperature and humidity sensing and 868 MHz RF transmitter module (STM 330 & HSM100, EnOcean GmbH, Germany) from which the solar cell, battery, and capacitor were removed and replaced with a 136 μF capacitor connected to the plants using the indicated circuits for energy harvesting, sensing, and data transmission.

High-speed camera recordings and analysis: The motion of each artificial leaf design was recorded at a frame rate of 600 fps using a Phantom Miro C110 (Phantom Ametek, New Jersey, USA). Analysis of the motion was done using the open-source software Tracker, version 6.1.5.

Data analysis: Information on data acquisition and statistics are given in the figure captions. Typically, the data points or curves represent mean and standard deviations of at least 3 measurements. All other experiments have been repeated multiple times, when single measurement data is shown, it is representative. Boxplots were chosen to represent data containing many data points (typically between 10 and 100), where the lower and upper edge of the box represent the 25th and 75th percentile, the middle line indicates the median (or 50th percentile) and the bars span from the minimum to the maximum value of the data. The statistical analysis was done in MATLAB (Version 2022b).

Data availability statement

The data that support the findings of this study are openly available at the following URL/DOI: https://doi.org/10.48557/YOQGW5.

Acknowledgments

The authors acknowledge funding by the Project GrowBot, the European Union's Horizon 2020 Research and Innovation Programme under Grant Agreement No. 824074. Fabian Meder acknowledges funding from the Freiburg Rising Star Academy. Thomas Speck is grateful for funding by the Deutsche Forschungsgemeinschaft (DFG, German Research Foundation) under Germany's Excellence Strategy—EXC-2193/1–390951807. We thank Marc Thielen for his help and support during the experiments at the Botanical Garden of University of Freiburg.

ORCID iDs

Fabian Meder https://orcid.org/0000-0002-1331-0265
Serena Armiento https://orcid.org/0000-0002-0318-4250
Giovanna Adele Naselli https://orcid.org/0000-0003-1849-9826
Alessio Mondini https://orcid.org/0000-0002-2303-2844
Thomas Speck https://orcid.org/0000-0002-2245-2636
Barbara Mazzolai https://orcid.org/0000-0003-0722-8350

References

[1] Dufil G, Bernacka-Wojcik I, Armada-Moreira A and Stavrinidou E 2022 Plant bioelectronics and biohybrids: the growing contribution of organic electronic and carbon-based materials *Chem. Rev.* **122** 4847–83
[2] Giraldo J P, Wu H, Newkirk G M and Kruss S 2019 Nanobiotechnology approaches for engineering smart plant sensors *Nat. Nanotechnol.* **14** 541–53
[3] Thomas T *et al* 2020 Species-independent analytical tools for next-generation agriculture *Nat. Plants* **6** 1408–17
[4] Lee G, Wei Q and Zhu Y 2021 Emerging wearable sensors for plant health monitoring *Adv. Funct. Mater.* **31** 2106475
[5] Diacci C *et al* 2021 Diurnal *in vivo* xylem sap glucose and sucrose monitoring using implantable organic electrochemical transistor sensors *iScience* **24** 101966
[6] Fiorello I, Meder F, Mondini A, Sinibaldi E, Filippeschi C, Tricinci O and Mazzolai B 2021 Plant-like hooked miniature machines for on-leaf sensing and delivery *Commun. Mater.* **2** 103
[7] Jiang J, Zhang S, Wang B, Ding H and Wu Z 2020 Hydroprinted liquid-alloy-based morphing electronics for fast-growing/tender plants: from physiology monitoring to habit manipulation *Small* **16** 2003833
[8] Khan S M, Shaikh S F, Qaiser N and Hussain M M 2018 Flexible lightweight CMOS-enabled multisensory platform for plant microclimate monitoring *IEEE Trans. Electron Devices* **65** 5038–44
[9] Bernacka-Wojcik I *et al* 2023 Flexible organic electronic ion pump for flow-free phytohormone delivery into vasculature of intact plants *Adv. Sci.* **10** 2206409
[10] Graule M A, Chirarattananon P, Fuller S B, Jafferis N T, Ma K Y, Spenko M, Kornbluh R and Wood R J 2016 Perching and takeoff of a robotic insect on overhangs using switchable electrostatic adhesion *Science* **352** 978–82
[11] Jiaming L *et al* 2021 Electrostatic footpads enable agile insect-scale soft robots with trajectory control *Sci. Robot.* **6** eabe7906
[12] Kocer B B *et al* 2021 Forest drones for environmental sensing and nature conservation *2021 Aerial Robotic Systems Physically Interacting with the Environment (AIRPHARO)* (IEEE) pp 1–8
[13] Shaikh F K and Zeadally S 2016 Energy harvesting in wireless sensor networks: a comprehensive review *Renew. Sustain. Energy Rev.* **55** 1041–54
[14] Meder F, Thielen M, Mondini A, Speck T and Mazzolai B 2020 Living plant-hybrid generators for multidirectional wind energy conversion *Energy Technol.* **8** 2000236
[15] Meder F, Armiento S, Naselli G A, Thielen M, Speck T and Mazzolai B 2021 Biohybrid generators based on living plants and artificial leaves: influence of leaf motion and real wind outdoor energy harvesting *Bioinspir. Biomim.* **16** 055009
[16] Wu H, Chen Z, Xu G, Xu J, Wang Z and Zi Y 2020 Fully biodegradable water droplet energy harvester based on leaves of living plants *ACS Appl. Mater. Interfaces* **12** 56060–7
[17] Meder F, Mondini A, Visentin F, Zini G, Crepaldi M and Mazzolai B 2022 Multisource energy conversion in plants with soft epicuticular coatings *Energy Environ. Sci.* **15** 2545–56

[18] Helder M, Strik D P B T B, Hamelers H V M, Kuhn A J, Blok C and Buisman C J N 2010 Concurrent bio-electricity and biomass production in three Plant-Microbial Fuel Cells using Spartina anglica, Arundinella anomala and Arundo donax *Bioresour. Technol.* **101** 3541–7
[19] Xu Y, Lu Y and Zhu X 2021 Toward plant energy harvesting for 5G signal amplification *ACS Sustain. Chem. Eng.* **9** 1099–104
[20] Maddalwar S, Kumar Nayak K, Kumar M and Singh L 2021 Plant microbial fuel cell: opportunities, challenges, and prospects *Bioresour. Technol.* **341** 125772
[21] Flexer V and Mano N 2010 From dynamic measurements of photosynthesis in a living plant to sunlight transformation into electricity *Anal. Chem.* **82** 1444–9
[22] Miyake T, Haneda K, Nagai N, Yatagawa Y, Onami H, Yoshino S, Abe T and Nishizawa M 2011 Enzymatic biofuel cells designed for direct power generation from biofluids in living organisms *Energy Environ. Sci.* **4** 5008–12
[23] Mano N, Mao F and Heller A 2003 Characteristics of a miniature compartment-less Glucose−O_2 biofuel cell and its operation in a living plant *J. Am. Chem. Soc.* **125** 6588–94
[24] So C P *et al* 2016 On harvesting energy from tree trunks for environmental monitoring *Int. J. Distrib. Sens. Netw.* **12** 9383765
[25] Himes C, Carlson E, Ricchiuti R J, Otis B P and Parviz B A 2010 Ultralow voltage nanoelectronics powered directly, and solely, from a tree *IEEE Trans. Nanotechnol.* **9** 2–5
[26] Meder F *et al* 2018 Energy conversion at the cuticle of living plants *Adv. Funct. Mater.* **28** 1806689
[27] Armiento S, Filippeschi C, Meder F and Mazzolai B 2022 Liquid-solid contact electrification when water droplets hit living plant leaves *Commun. Mater.* **3** 79
[28] Meder F, Naselli G A and Mazzolai B 2022 Wind dynamics and leaf motion: approaching the design of high-tech devices for energy harvesting for operation on plant leaves *Front. Plant Sci.* **13** 994429
[29] Jie Y, Jia X, Zou J, Chen Y, Wang N, Wang Z L and Cao X 2018 Natural leaf made triboelectric nanogenerator for harvesting environmental mechanical energy *Adv. Energy Mater.* **8** 1703133
[30] Armiento S, Mondini A, Meder F and Mazzolai B 2022 A plant-hybrid system for wind monitoring connected with social media *2022 IEEE 5th Int. Conf. on Soft Robotics (Robosoft)* (IEEE) pp 287–92
[31] de Baar J H S, van der Schrier G, van den Besselaar E J M, Garcia-Marti I and de Valk C 2023 A new E-OBS gridded dataset for daily mean wind speed over Europe *Int. J. Climatol.* **43** 6083–100
[32] Tadrist L *et al* 2018 Foliage motion under wind, from leaf flutter to branch buffeting *J. R. Soc. Interface* **15** 20180010
[33] Meder F 2024 Replication data for: Charge generation by passive plant leaf motion at low wind speeds: design and collective behavior of plant-hybrid energy harvesters IIT Dataverse, V1 (https://doi.org/10.48557/YOQGW5)
[34] Zhao C, Hu G and Yang Y 2022 A cantilever-type vibro-impact triboelectric energy harvester for wind energy harvesting *Mech. Syst. Signal Process.* **177** 109185
[35] Pecunia V, Occhipinti L G and Hoye R L Z 2021 Emerging indoor photovoltaic technologies for sustainable internet of things *Adv. Energy Mater.* **11** 2100698